

Preliminary neutronics optimization on the concept of multi-beam accelerator driven system

Xunchao Zhang ^{a,b}, Neng Pu ^a, Huan Jia ^{a,b}, Yuanshuai Qin ^{a,b}, Hanjie Cai ^{a,b}, Yuan He ^{a,b,*}

^a Institute of Modern Physics, Chinese Academy of Sciences, Lanzhou, 730000, China

^b University of Chinese Academy of Sciences, Beijing, 100049, China



ARTICLE INFO

Keywords:
Accelerator-driven system
Beam splitting
Neutronics
Spallation target

ABSTRACT

A new subcritical reactor concept is proposed as one accelerator beam splitting into multiple beams to drive the subcritical reactor in this work, which is so called Multi-Beam Accelerator Driven System (MB-ADS). The spallation target is designed as a target assembly to the fuel assembly. The high current proton beam is divided into multiple parts and injected into different targets scattered among the core to improve the beam efficiency and flatten the spatial power distribution of the core. Based on different MB-ADS schemes, neutronics were conducted on the effects of splitting beam number, target assembly arrangements, fuel zoning, and neutron data libraries. The results show that a reasonable multi-beam scheme can significantly improve the efficiency of the proton beam and flatten the power distribution of the reactor compared to the one target ADS scheme. With the improved beam efficiency, the beam density on the target window is greatly reduced.

1. Introduction

Accelerator Driven System (ADS) is aimed at transmuting the long-lived radioactive isotopes in the spent nuclear fuels into fission products with shorter half-lives. The power level of the industrial grade sub-critical reactor is usually above hundreds of megawatts for efficient transmutation; and the corresponding proton beam power has also reached tens of megawatts. For instance, the European Facility for Industrial-scale Transmutation (EFIT) concept has a thermal power of 400 MW with the proton beam power of 16 MW (Mansani et al., 2012; Pignatelli et al., 2012), and the ADS investigated by JAEA is a Lead Bismuth Eutectic (LBE) cooled sub-critical reactor with 800 MW thermal power and proton beam power of 22.5 MW (Tsujimoto et al., 2004). In the design scheme of ADS plant with one target, high-intensity external neutrons are concentrated in the center of the core which will result in a high-power peak factor.

The Energy Amplification Factor (EAF) is defined as the ratio of core thermal power (P_f) to beam power (P_b). The EAF can be a criterion for evaluating the beam efficiency in ADS design. The accelerator cost and operation and maintenance expenses depend on the beam power, so a low beam efficiency will inevitably lead to an increase in the cost of the ADS. In addition, beam efficiency has also determined the proton beam demand, which in turn determines the difficulty of design and operation

the spallation target. Appropriately increasing the k_{eff} of sub-critical reactor is a method to increase beam efficiency. In the design of the JAEA-ADS and ANL-ADS, the k_{eff} of the reactor is 0.98 (Gohar et al., 2021; Sugawara et al., 2018).

The scheme that the beam pipe directly inserted into the core is adopted in the design of JAEA-ADS and MYRRHA spallation targets because LBE is core coolant and at the same time can be a target material, where the front end of the beam pipe is the target window (Sugawara et al., 2018; Abderrahim et al., 2012; Keijers, 2014). The proton beam passes through the target window and directly bombards the LBE coolant in the core to generate spallation neutrons. The beam heat deposited on the target window and coolant can be removed by the heat removal system. This design combines the spallation target and the reactor with one heat removal system, reducing most of the conventional target equipment and simplifying the ADS. In design of MYRRHA, the spallation target is designed as a target assembly that can be conveniently placed in different positions in the core (Keijers, 2014). The concept of multiple spallation target-driven ADS was proposed in the early years for flattening the core power distribution and reducing the probability of long interruption of beam time (Dagan and Broeders, 1999; Ali et al., 2013). Previous studies adopted the scheme of three targets and three accelerators, where each spallation target and accelerator had independent equipment systems. This scheme has to some

* Corresponding author. Institute of Modern Physics, Chinese Academy of Sciences, Lanzhou, 730000, China.

E-mail address: hey@impcas.ac.cn (Y. He).

Data Source	Nuclides (200 MeV)	Temperatures (K)
JENDL-5	^{1}H , ^{2}H , ^{12}C , ^{13}C , ^{16}O , ^{17}O , ^{18}O , ^{14}N , ^{15}N , ^{28}Si , ^{29}Si , ^{30}Si , ^{46}Ti , ^{47}Ti , ^{48}Ti , ^{49}Ti , ^{50}Ti , ^{51}V , ^{58}Fe , ^{59}Fe , ^{54}Cr , ^{53}Cr , ^{52}Cr , ^{64}Ni , ^{60}Ni , ^{61}Ni , ^{94}Zr , ^{92}Zr , ^{91}Zr , ^{90}Zr , ^{55}Mn , ^{98}Mo , ^{95}Mo , ^{97}Mo , ^{100}Mo	294, 600, 900, 1200, 1500, 2500
TENDL-2021	^{20}Pb , ^{205}Pb , ^{207}Pb , ^{208}Pb , ^{209}Bi , ^{238}U , ^{237}Np , ^{238}Pu , ^{239}Pu , ^{240}Pu , ^{241}Pu , ^{242}Pu , ^{241}Am , ^{242}Am , ^{243}Cm , ^{244}Cm , ^{245}Cm , ^{246}Cm , ^{243}Am , ^{242}Cm	

extent flattened the core power, but it also brings complex challenges to the system.

In order to further improve the beam efficiency, flatten core power, and reduce the complexity of spallation targets. In this work, we consider dividing one proton beam into multiple sub-beams with only one accelerator and using more compact target assembly to drive the sub-critical reactor. The beam splitting system (BSS) includes some segments as follows: RF cavity deflecting, quadrupoles focusing, septum magnets bending, double-circle scanning and SC bending. Direct Current (DC) proton beam is bunched by a Radio Frequency Quadrupole (RFQ), and the period between adjacent bunches is 6.15 ns? The RMS phase length of the bunch extends naturally from 0.2° to 5° in HEBT, which is short enough for beam splitting with RF cavities without losing significant beam quality. With this strategy, the proton beam can be injected into the core more finely and uniformly. The present work seeks to optimize the number of sub-beams and the layout of the target assemblies through simulations.

2. Calculation methods and models

2.1. Simulation codes and neutron libraries

The two-steps method is adopted to the neutronics calculations of ADS(Pu a et al., 2023). For the first step, PHITS (Particle and Heavy Ion Transport code System) is used to simulate the transport process of proton beam in LBE coolant to generate the external neutron source information for subcritical reactor neutronics calculations. It can deal with the transport of most particles over wide energy ranges, using several nuclear reaction models and nuclear data libraries (Sato et al., 2018). In the second step, OpenMC-0.13.0 is used to simulate the neutronics of subcritical reactor driven by external neutron source generated from PHITS. OpenMC is a community-developed Monte Carlo neutron and photon transport simulation code (Romano et al., 2015). It is capable of performing fixed source, k-eigenvalue, and sub-critical multiplication calculations.

The neutron cross section plays an important role in ADS neutronics calculations, especially the high-energy neutron(>20 MeV) cross section has a great influence on the beam driving efficiency (Pu a et al., 2023). Njoy21(Conlin, 2019) and OpenMC was used to process a continuous energy neutron HDF5 format library with an energy upper limit of 200 MeV for OpenMC based on JENDL-5 (Iwamoto et al., 2023) and TENDL-2021 (Koning et al., 2019). JENDL-5 increases neutron reaction data in the number of nuclides up to 795, and extends some of the nuclides' energy region to 200 MeV. Because there are not enough nuclides with 200 MeV in JENDL-5, the rest is replenished by nuclides from TENDL-2021 as shown in Table 1. This work mainly studies the neutronics at the initial time of the subcritical reactor, so only the neutron data energy of nuclide in the model is guaranteed to be up to 200 MeV. In order to compare the preliminary differences from high-energy neutron effects in a same library and cross-section libraries, ENDF/B-VII.1, ENDF/B - VII.0, and JEFF-3.3 were also used in the calculation of the selected optimization schemes.

2.2. Sub-critical reactor model

A Multi-Beam Accelerator Driven Sub-critical conceptual Reactor (MB-ADS) is established as shown in Fig. 1. The core is a LBE cooled fast reactor with a thermal power of 1500 MW, and the detailed parameters is given in Table 2. The conceptual design of the core refers to the design of Russian lead cooled reactor BREST-OD-1200 (Bokova et al., 2021) and JAEA-ADS, and the core is filled with transmutation fuel. The height of the fuel active zone is set to 150 cm to improve the efficiency of external neutrons. The long fuel region reduces the leakage rate of external neutrons from both ends of the target.

The proton beam energy is 1.0 GeV. The proton beam generated by one accelerator will be divided into multiple beams and injected into the

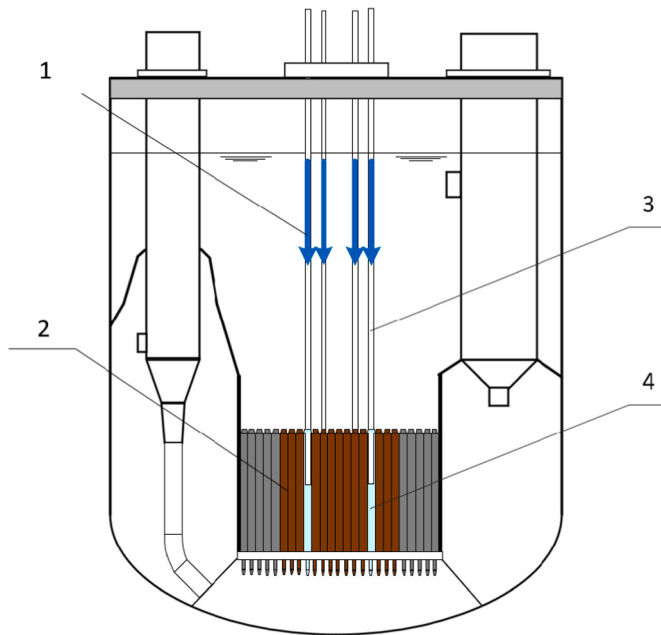


Fig. 1. Multi-beam accelerator driven sub-critical reactor.

core along each beam pipes. The spallation target of this scheme is different from the conventional ADS spallation target. It is designed as a target assembly similar to the fuel assembly, the front end of the beam pipe is connected with the target window and penetrates into the target assembly as shown in Fig. 1. The target assembly is fixed on the grid plate at the lower end of the core as the fuel assembly. There are no control sub-assemblies in the core, and the power control of MB-ADS is achieved by adjusting the proton beam current. During the operation of a sub-critical reactor, the k_{eff} remains below 0.98. Once the beam is cut off, the reactor can be shut down.

The Mixture of mono-nitride of minor actinides (MAs, including neptunium, americium, and curium) and plutonium (Pu) is used as fuel. The isotopic composition of MAs and Pu is recovered from the light water reactor (LWR) spent fuel. The zirconium-nitride (ZrN) is used as an inert matrix with the fuel. Nitrogen with ^{15}N enriched (100%) is assumed to be used for both (MAs, Pu)-nitride and ZrN. Table 3 shows the mass ratio of transuranic (TRU) nuclide, the mass ratio of Pu to MAs is about 4:6. Zirconium nitride accounts for 68.8% of mass fraction in the fuel.

2.3. Compact spallation target assembly

The concept of compact spallation target assembly (CSTA) is shown in Fig. 2-a. The shell structure of CSTA is the same as the fuel assembly. The side length of CSTA is 10.85 cm, and the diameter of beam pipe is 15.0 cm. The beam pipe is inserted into the CSTA from top of the core. The height of the target window is located near the center of the active region.

Compared to the Traditional ADS Spallation Target (TST), CSTA does not have an independent heat exchange circuit, and the target diameter is smaller (<20 cm). The same heat exchange system is used for both CSTAs and core. After passing through the target window, high-energy protons bombard lead and bismuth nuclei to generate spallation neutrons, and the power of the beam is deposited and taken away with the core coolant. At the same time, heat deposited in the target window is carried off with the flowing of coolant.

This work is devoted to search a reasonable number and arrangement of CSTAs in the core through simulations, and to obtain high beam efficiency and low peak factor of the reactor.

Table 2

The basic specifications of MB-ADS.

MB-ADS parameters	
Thermal Power (MWt)	1500
BOL- k_{eff}	~0.975
Coolant	LBE
Structural material	T91
Active core height (cm)	150.0
Reactor core diameter(cm)	~358.0
Average power density (W/cm ³)	~100
Assembly geometry	Hexagonal
Number of rods per assembly	127
Fuel pin diameter (cm)	1.04
Fuel element pitch (cm)	1.56
Number of fuel assemblies	~319
Reactor Fuel type	(Pu + MA)N-ZrN
Target assembly and proton beam parameters	
Proton energy(MeV)	1000
Number of target assemblies	>3
Beam pipe diameter(cm)	15.0
Beam diameter(cm)	12.0 (Uniform circular beam spot distribution)
Target window material	T91
Target window shape	Hemispherical shell

2.4. Calculation of neutronic parameters

OpenMC has a flexible, low-overhead tally system which enables users to obtain physical results of interest. The external neutron efficiency, which denoted as φ^* represents the relative efficiency of one external neutron. It is also the ratio of averaged importance of the one external neutron and one fission neutron. The external neutron efficiency can be expressed as:

$$\varphi^* = \frac{f\nu}{S} \left(\frac{1}{k_{\text{eff}}} - 1 \right) \quad (1)$$

Where, k_{eff} is the effective multiplication factor of the reactor, the total production of neutrons by fission ($f\nu$) is equal to fission rate (f) multiplied by the average number of fission neutrons per fission event(ν), and S is the external neutron intensity. The thermal power of reactor P_f can be expressed as the total number of fission neutrons according to the following equation:

$$P_f = Q \times f = \frac{Q\varphi^* S}{\nu} \left(\frac{k_{\text{eff}}}{1 - k_{\text{eff}}} \right) \quad (2)$$

where, P_f is the fission power of reactor, E_b is the energy of proton beam particle, Q is the average energy released per fission. The power of the proton beam P_b can be expressed as follows:

$$P_b = I \times E_b = \frac{S \times E_b}{z} \quad (3)$$

where, I is the proton beam current, and it is equal to the external neutron intensity (S) divided by the leakage neutron yield (z) by a proton injected in the target. Thus, EAF can be obtained as the following equation:

Table 3
ADS fuel nuclide composition of MAs and Pu (wt.%).

Nuclide	Mass Fraction (wt. %)	Nuclide	Mass Fraction (wt. %)
^{238}Pu	1.473	^{237}Np	25.46
^{239}Pu	21.54	^{241}Am	24.51
^{240}Pu	3.751	^{242m}Am	0.905
^{241}Pu	8.499	^{243}Am	7.615
^{242}Pu	4.74	^{244}Cm	2.178
Total Pu	40.0	Total MAs	60.0

*: Note that MA and Pu were recovered from the spent LWR fuel of 50 GWd/t burnup after 5 years cooling.

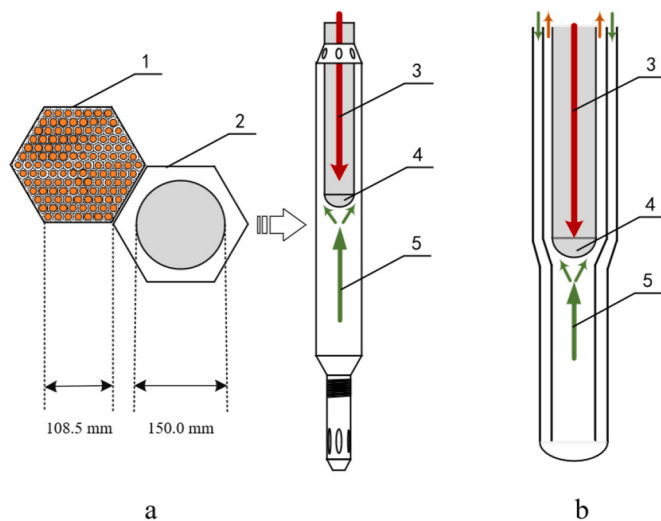


Fig. 2. The configuration of compact spallation target assembly (a) and traditional spallation target(b).

$$\text{EAF} = \left(\frac{z}{E_b} \right) \times \varphi^* \times \left(\frac{Qk_{\text{eff}}}{\nu(1 - k_{\text{eff}})} \right) \quad (4)$$

Here z/E_b represents the number of leaked neutrons produced by per unit energy proton bombarding the target. φ^* is not only related to the external neutron energy, but also to the coupling structure between the spallation target and the reactor. In the simulations of neutronics, f_V can be obtained by the Nu-Fission Rate tally filter and the fission power induced by external neutrons can be given by the Kappa-Fission Rate provided by OpenMC code.

3. Results and discussion

3.1. External neutron source

First, the PHITS code is employed to simulate the proton transport process within the spallation target in order to acquire information regarding the external source neutrons. The target is a cylinder with a length of 100 cm, and the radii are 15 cm, 20 cm, 30 cm, 45 cm, 50 cm and 60 cm with hemispherical beam windows to study relation of

neutron yield with target sizes. The neutron source generated by a target diameter of 15 cm was used in the MB-ADS simulations. The leakage neutron information from the spallation target will be recorded, encompassing position coordinates, energy, weight and direction vectors. This data will be stored in HDF5 files to facilitate coupling with OpenMC calculations.

Fig. 3-a shows the total yield of leaked neutrons from the surface of the target as a function of target diameter. At the same time, it also provides the fraction variation of the leaked neutrons emitted from the recoil, forward and lateral surfaces with respect to the target diameter. As the diameter of the target increases, high-energy neutrons react through (n, xn) to produce more leakage neutrons, but more collisions also cause a decrease in leakage neutron energy (Zhang et al., 2019). It is worth noting that neutrons emitted from the upper and lower surfaces of the target are prone to escape sub-critical, resulting in lower neutron efficiency. The lateral leakage neutron yield did not increase with the increase of target diameter, and it begins to show a decreasing trend when the target diameter exceeded 40 cm.

The energy of the spallation neutrons produced by proton bombardment on target is significantly different from that of the fission neutrons. Most fission neutrons have energies between 0.1 MeV and 10 MeV, while the energy of a spallation neutron can reach up to 1 GeV. The upper limit of neutron energy for most nuclear evaluation libraries is 20 MeV, and only some nuclides have neutron energies up to 200 MeV. It can be seen from **Fig. 3-b** that fission neutron yield of actinide nuclides is closely related to the incident neutron energy. When the incident neutron energy exceeds 5 MeV, the fission neutron yield increases with the increase of the incident neutron energy.

We divide the leakage neutrons into five energy groups according to the energy upper limit of the neutron library and the fission neutron yield spectrum. **Table 4** shows the distribution information of leakage neutrons in different energy groups. The leakage neutron yield increases with the increase of target diameter. Most of the leaked neutrons are concentrated and almost the same with increase of target diameter between 0.1 MeV and 5 MeV, and low energy neutrons (<0.1 MeV) are increasing with the increase of target diameter, and the fraction of high-energy neutrons (>20 MeV) decreases significantly with the increase of target diameter. When the diameter of target is less than 20 cm, the share of high-energy neutrons even exceeds 6%, neutrons above 200 MeV account for 1%.

It should be pointed out that the processing of neutrons with energies greater than 20 MeV will have a significant impact on the beam

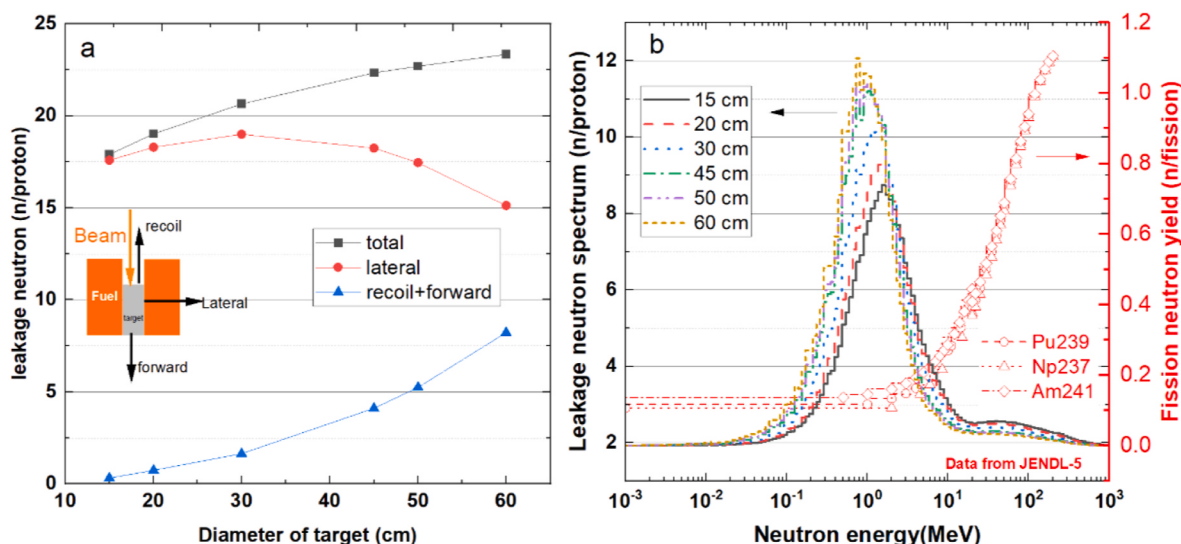


Fig. 3. Leakage neutron yields of standard spallation target with different diameters(a); the fission neutron yield of actinide nuclide with incident neutron energy, and the leakage neutron spectrum (b).

Table 4

Distribution of leaked neutrons in different energy groups.

Target diameter (cm)	<S> (n/proton)	Average energy (MeV)	Energy group (MeV)				
			<0.1	0.1~5	5~20	20~200	>200
15	17.91	12.32	1.25%	80.19%	10.17%	7.17%	1.21%
20	19.03	9.97	1.47%	82.94%	8.69%	6.00%	0.91%
30	20.63	7.36	1.92%	86.34%	6.59%	4.56%	0.59%
45	22.35	5.28	2.72%	88.97%	4.69%	3.24%	0.38%
50	22.74	4.84	3.03%	89.42%	4.25%	2.96%	0.34%
60	23.97	4.20	3.69%	89.92%	3.58%	2.53%	0.28%

efficiency. Although the proportion of high-energy neutrons in the leakage spallation neutron is only a few percent, it has an impact on the beam current of more than 20% (Pu a et al., 2023; Zheng et al., 2017). This is because the fission of actinide induced by high-energy neutrons can release more fission neutrons as shown in Fig. 3-b. The neutron efficiency of 100 MeV neutron is tens of times higher than that of 0.1 MeV neutron (Pu a et al., 2023). It can be seen that under a fixed k_{eff} , the beam efficiency is mainly determined by the relative efficiency of one external neutron (φ^*) and the leakage neutron yield (z). Therefore, simulations are needed to obtain a precise conclusion on the relationship between the beam efficiency and the variation in the diameter of the target. Based on the current neutron data libraries, the upper limit of neutron energy can only reach 200 MeV. The energy will be unified as 200 MeV in simulations for the neutrons higher than 200 MeV.

3.2. The neutronics characteristics of one target ADS

For conventional ADS, the spallation target is located in the center of the core. In this section, we will discuss the neutronics characteristics of the sub-critical reactor driven by one target with target diameter effect on beam efficiency and power distribution in core.

There are four sub-critical reactor schemes as shown in Fig. 4. CSTA-1 is one CSTA scheme, and TST-1, TST-2-a and TST-2-b are traditional target schemes with different target diameters. In the TST-1 and TST-2 scheme, 7 and 19 fuel assemblies (FA) are extracted from the center of the core, respectively. In the TST-2 scheme, the a-core fuel is uniformly fuel arranged and the b-core is arranged in inner and outer zones with different FAs. The diameter of fuel rod in the outer zone is larger than that in the inner zone for power flattening. The reflection assemblies (RA) are arranged outside of the FA.

Table 5 shows the main neutronics results of the four schemes. The k_{eff} of those sub-critical reactors is set between 0.978 and 0.979, and the statistical error of the results is about 20 pcm. It can be seen that the average efficiency of one external neutron decreases with the increase of target diameter. The increase in the diameter of the target can also lead to an increase in neutron leakage in the direction of beam recoil and forward, resulting in a decrease in the efficiency of external neutrons. The simulation results show that in the CSTA scheme, due to the high energy of leaked neutrons and low core axial neutron leakage rate, the efficiency of a single external neutron reaches 2.04. In the TST-2 scheme, due to the low energy of leaked neutrons and an increase in neutron leakage in the direction of beam recoil, resulting in a decrease in the efficiency of a single external neutron to 0.84. Normalized with a fixed fission power of reactor, the proton beam current increase with the decrease of the beam efficiency.

The beam density can be obtained by dividing the beam current by the beam spot area. The calculated beam densities are also given in Table 5 based on the premise of circular uniform proton beam. The ratio of beam pipe to target diameter refers to the design of ADTF proposed by ANL (Gohar et al., 2002). In this work, the density of proton beam is used as the judgement for challenge of target. Because the beam density affects the thermal hydraulic design and radiation damage evaluation of the target window. In many ADS designs with window targets, the beam density is generally limited to $20 \mu\text{A}/\text{cm}^2 \sim 40 \mu\text{A}/\text{cm}^2$ (Gohar et al.,

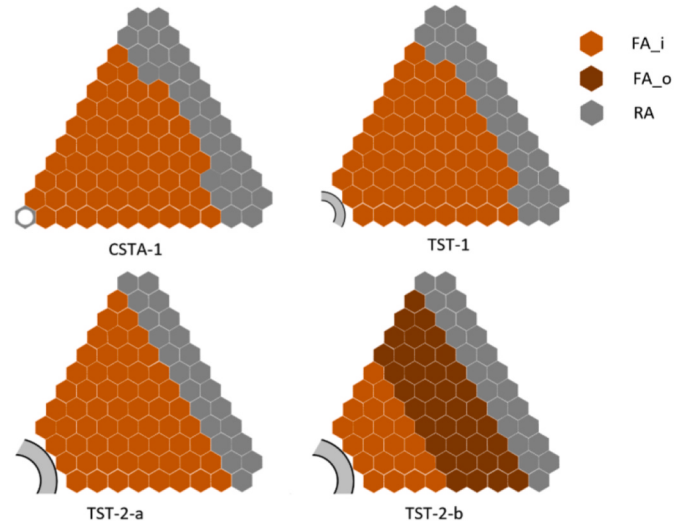


Fig. 4. Four schemes of sub-critical reactor driven by one target.

2021; Sugawara et al., 2018; Keijers, 2014; Gohar et al., 2002). It is limited by the velocity of LBE/lead coolant and the radiation damage of window material caused by proton beam. Although the beam current in CSTA and TST-1 schemes is low, the small beam pipe diameter leads to the beam density of $119.96 \mu\text{A}/\text{cm}^2$ and $54.02 \mu\text{A}/\text{cm}^2$. In contrast, the use of larger diameter targets in the TST-2 scheme increases the beam current. However, due to the larger beam pipe, the beam density decreased to about $23 \mu\text{A}/\text{cm}^2$.

The strategy of fuel zoning is often used to flatten the core power, and make the FAs around the spallation target to meet the thermal and hydraulic limits. The beam current is higher than that in TST-2-a scheme when the fuel zoning arrangement is adopted in TST-2-b scheme. From Fig. 7 in Chapter 3.3.1, it can be seen that the efficiency of one external neutron in the center of the core is higher under the scheme of uniform fuel arrangement than that of fuel zoning scheme. The ADS scheme for a single target emits its external neutrons from the center of the core. Therefore, the adoption of fuel zoning strategy in the single-target ADS scheme will lead to a reduction in the beam efficiency.

Fig. 5 shows the radial power density distributions of the fuel pins in the axial center of the FAs under different schemes. According to the symmetry of the FA near the target, we choose horizontal and vertical directions to tally the heat deposition in fuel pins. A small diameter spallation target leads to a strong neutron emission density. Therefore, the power density around the small diameter spallation target will be high. The peak power density in the CSTA-1 exceeded $1500 \text{ W}/\text{cm}^3$. The maximum power density in fuel pin decreases to $1200 \text{ W}/\text{cm}^3$ and $1000 \text{ W}/\text{cm}^3$ from TST-1 scheme to TST-2-a scheme with the increase of target diameter. It can be seen from Fig. 5 that the radial power density of the core has been slightly flattened after TST-2-b adopted the fuel zoning arrangement, and the maximum power density in the fuel pin has decreased by about $100 \text{ W}/\text{cm}^3$ comparing to TST-2-a.

In the design of industrial ADS, the limitations radiation damage of

Table 5

Basic parameter setting and simulation results based on those schemes of single spallation target driven sub-critical reactor.

Parameters	CSTA	TST-1	TST-2-a	TST-2-b
Reactor power (MWt)	1500			
k_{eff}	0.97811	0.97894	0.97871	0.97887
Target diameter (cm)	18	40	67.6	67.6
Beam diameter (cm)	12	20.5	36.7	36.7
Number of FA	300	306	312	312
Beam current (mA)	13.56	17.82	22.11	24.36
Neutron efficiency(φ^*)	2.04	1.53	0.93	0.84
Beam density($\mu\text{A}/\text{cm}^2$)	119.96	54.02	20.91	23.04
Beam efficiency (EAF)	110.62	84.17	67.84	61.57

target window and the thermal and hydraulic of FA near the target are important issues. Although the strategy of fuel zoning is conducive to flattening the core power peak, it also increases the beam current. The diameter of spallation target has to increase to meet the constraints of thermal and material. Therefore, the beam current will also increase, leading to an increase in the cost of the accelerator itself and a decrease in the system's productivity efficiency.

3.3. Neutronic optimization of MB-ADS

Through the discussion in section 3.2, it is known that the beam efficiency of the CSTA with smaller diameter is higher. We expect to arrange a reasonable number of CSTAs in reasonable positions of the core to improve the beam efficiency and flatten the power of the core.

3.3.1. Effect of CSTA position on neutron efficiency

The correlation between CSTA position and external neutron efficiency is related to its position in the core. For this study, two core arrangements are selected as shown in Fig. 6, one is uniform fuel arrangement (Case-1), and another is fuel zoning arrangement (Case-2). There are ten positions(A~J) of CSTA from the inside to outside. In the following simulations, the external neutrons will emit from different positions A to J in sequence to obtain the variation of neutron source efficiency. The k_{eff} of the cores of Case-1 and Case-2 are 0.97943 and 0.97852 when no CSTA is placed.

Fig. 7 shows the φ^* at different radial positions, where the horizontal axis A~J represents the position of CSTA in the core from inside to outside as shown in Fig. 6. In Case-1, the φ^* is the highest when the target is located in the center of the core. As the target position moving outward, the φ^* gradually decreases. In Case-2, the φ^* in the center region is significantly reduced, but the φ^* in the outer fuel region is improved. This explains why the target is placed in the center of the core to obtain the highest neutron efficiency in one target ADS. After power flattening using fuel zoning arrangement, the proton beam current increases due to the decrease of neutron efficiency. Therefore, the CSTA should be placed as close as possible to the center of the core.

3.3.2. Six-CSTA schemes

Firstly, let's study the impact of the distance between the CSTAs on neutronics. According to the geometric symmetry of the core arrangement of hexagonal FA, the study of six-CSTA scheme (CSTA-6) is considered. It is expected to get the neutronic influence of the distance

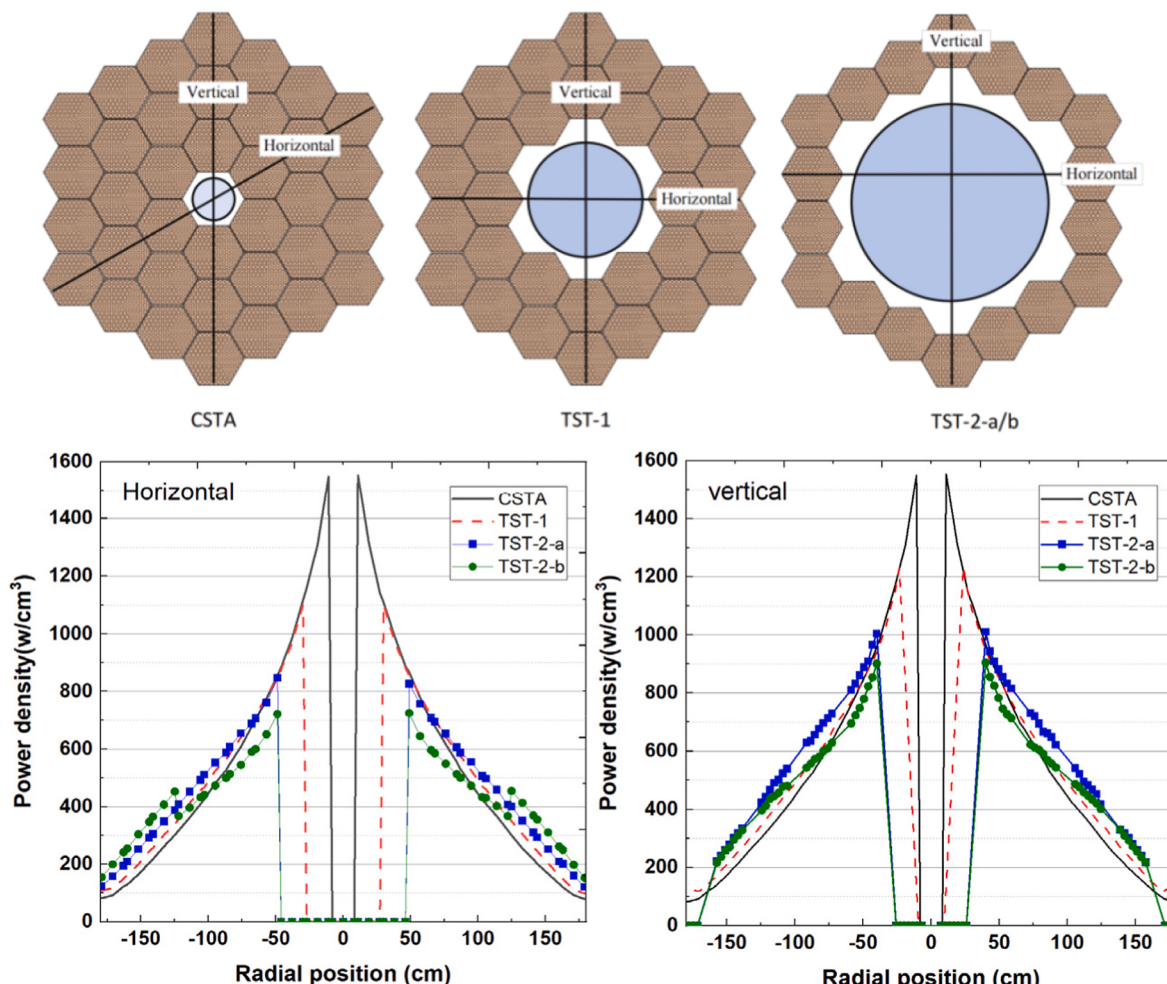


Fig. 5. Distributions of radial power density in horizontal and vertical directions.

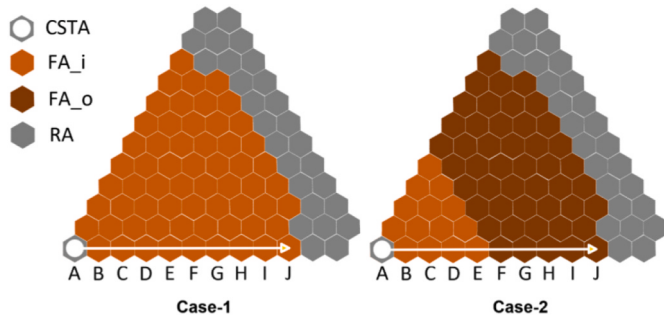


Fig. 6. Positions of the CSTA in neutron efficiency calculation under the uniform (Case-1) and zoning arrangement schemes (Case-2).

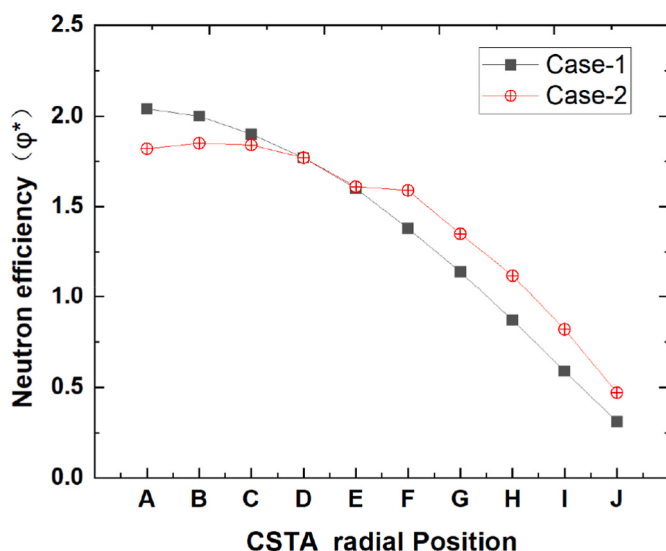


Fig. 7. Variation of external neutron efficiency with CSTA neutron source position.

between CSTAs and their positions in the core. As shown in Fig. 8, six CSTAs will be arranged along three diagonals of the core hexagon to change their distance to the core center.

The core k_{eff} is set between 0.978 and 0.979 under different schemes, and the statistical error is 20 pcm. The fission power of the core is 1500MWt under all schemes. Table 6 shows the calculated neutronics parameters of those schemes. The external neutron efficiencies of those schemes are all higher than that of the TST-2. The beam currents are lower than that of the TST-2 in the schemes of CSTA-6-1 to CSTA-6-4, in which the CSTAs are close to the core center. In schemes CSTA-6-5 and CSTA-6-6, the beam demand is high due to the placement of CSTAs in low neutron efficiency areas as shown in Fig. 7. After the multi-beam strategy is adopted, the beam density of CSTA-6-1 to CSTA-6-4 schemes has been significantly reduced compared to the TST-1. Under the CSTA-6-1 and CSTA-6-2 schemes, the beam density decreased from $110 \mu\text{A}/\text{cm}^2$ to about $20 \mu\text{A}/\text{cm}^2$ compared with the CSTA-1 scheme and that the beam current did not increase significantly.

The fuel pins with a length of 1 cm in the axial center of the FAs are chosen as the target of tally to study the radial distribution of heat deposition. The highest fuel power density and beam density in different schemes are shown in Fig. 9. The highest power density of fuel shows an opposite trend to the beam intensity. It is difficult to reduce the maximum power density of fuel and the beam density of window

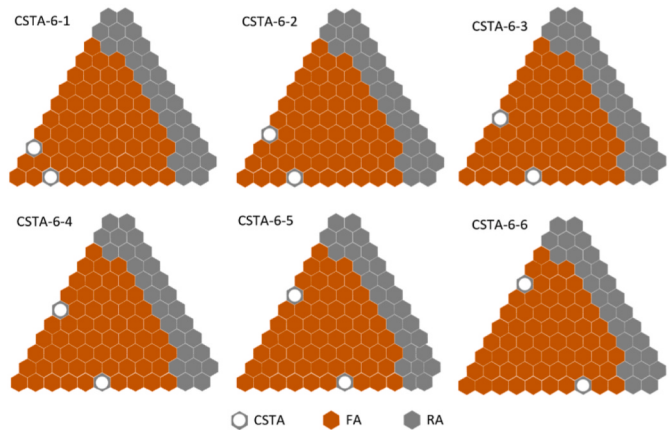


Fig. 8. Schematic diagrams of CSTA position under six-beam injection scheme.

simultaneously. The more reasonable scheme seems to be CSTA-6-4. Compared with TST-2-b scheme, the beam current is reduced by 28.6%, the maximum pin power density is reduced by about 18.8%, and the beam density is increased by $2 \mu\text{A}/\text{cm}^2$. It can be seen that a reasonable layout of CSTAs can simultaneously reduce the beam current and the power density of fuel pin. However, due to the relatively small beam irradiation area in 6-beam schemes, the beam density has not been significantly improved.

3.3.3. Twelve-CSTA schemes

The scheme optimization with twelve beams injected in 12 targets (CSTA-12) in the core is discussed in this section. The twelve CSTAs will be organized into two groups, each consisting of six CSTAs. They will be positioned symmetrically both inside and outside the core. The CSTAs layout of the inner ring follows the CSTA-6-2, CSTA-6-3, and CSTA-6-4 schemes in Fig. 8. The CSTAs in the outer ring will be placed at fixed positions. By this way, three schemes for uniformly fuel arrangement are obtained. Based on CSTA-12 scheme, the core is divided into internal and external zones to obtain another comparative scheme as shown in Fig. 10.

The neutronics parameters for the CSTA-12 schemes were obtained through simulations as shown in Table 7. The k_{eff} of core is set around 0.9785, and the statistical error is 20 pcm. Similarly, the fission power of the core is 1500MWt under all schemes. The proton beam currents in the CSTA-12 schemes have increased by approximately 4 mA compared with the CSTA-6 schemes. This is because there are six CSTAs arranged in the region of the core edge where the external neutron efficiency is reduced. It is worth noting that the beam currents under the schemes of fuel zoning arrangement are smaller than that of the uniform fuel arrangement schemes. As shown in Fig. 7, the neutron efficiency is decreased at the central position of the core by using the fuel zoning arrangement strategy, a smaller change in the neutron efficiency is observed in the transition region, and the neutron efficiency at the outer region increase overall.

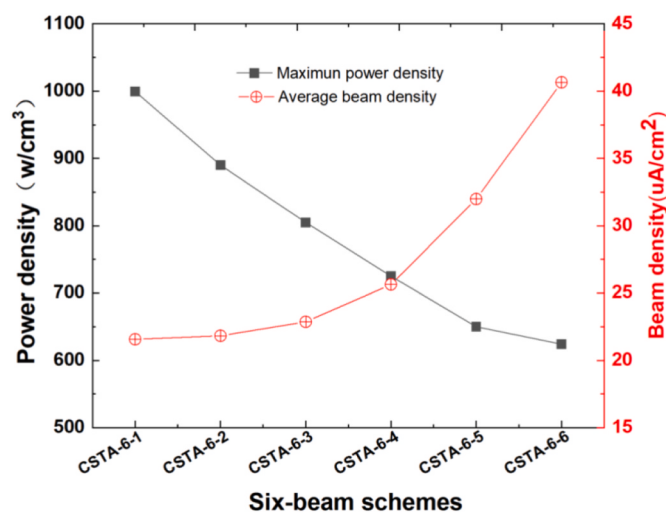
The external neutron efficiency of the CSTAs in the inner circle is basically not changed remarkably due to their departure from the center of the core. In the fuel zoning schemes, the external neutron efficiency of CSTAs arranged at the outer region has been improved as shown in Fig. 7. This is quite different from the TST-2 of ADS as mentioned in section 3.2. Therefore, the beam current of the scheme using fuel zoning strategy is reduced compared with the corresponding uniform fuel loading scheme.

As can be seen from Tables 6 and 7, the proton beam current has

Table 6

Neutronics parameters of the CSTA-6 schemes.

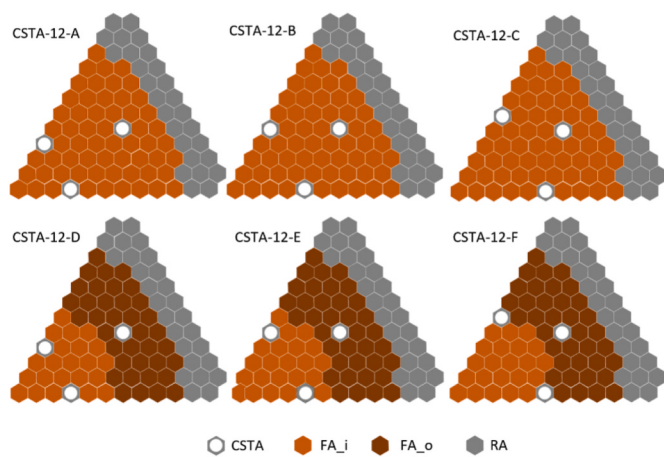
Case	k_{eff}	φ^*	Beam density ($\mu\text{A}/\text{cm}^2$)	Beam current (mA)	Beam efficiency (EAF)
CSTA-6-1	0.97868	1.84	21.57	14.63	102.5
CSTA-6-2	0.97825	1.86	21.84	14.81	101.3
CSTA-6-3	0.97878	1.73	22.87	15.51	96.7
CSTA-6-4	0.97876	1.54	25.64	17.39	86.2
CSTA-6-5	0.97823	1.27	31.99	21.70	69.1
CSTA-6-6	0.97846	0.99	40.66	27.57	54.4

**Fig. 9.** Comparison of maximum power density and beam density in the fuel pin.

increased by 5~20% in the CSTA-12 schemes compared to the CSTA-6-4 scheme, while the beam density has decreased by nearly 50%. Compared with TST-2-a and TST-2-b, the proton beam intensity of CSTA-12-F scheme is reduced by 14.9% and 22.7%, the beam efficiency is increased by 17.5% and 29.5%, and the beam density on the target window is reduced by 33.6% and 39.8%. It can be concluded here that the multi-beam driven subcritical reactor scheme has significant advantages over the one target ADS scheme in neutronics.

Fig. 11 presents the pin power distribution at axial center position of fuel rod. The results show that the radial power distribution is flatter in the scheme where CSTA is far from the core, and the peak power density of fuel pin can be significantly reduced in the fuel zoning strategy. In the uniformly distributed fuel core scheme, the highest pin power is located at the center of the core, while in the fuel zoning scheme, the highest fuel power density is located near CSTA.

The spatial distribution of pin power density in the CSTA-12 schemes is discussed in this part. The geometric spatial tally diagram is shown in Fig. 12. According to the symmetry of CSTA layout, the radial power distribution is selected in both horizontal and vertical directions, and the tally fuel pins are located in the axial center of each fuel rod. Two fuel assemblies have also been selected for the axial power distributions tally, the first location A being the FA in the center of the core, and the second location B being the FA adjacent to the CSTA.

**Fig. 10.** Schematic diagrams of MB-ADS under twelve-beam injection schemes.**Table 7**

Neutronics parameters of CSTA-12 schemes.

Position	k_{eff}	φ^*	Beam density ($\mu\text{A}/\text{cm}^2$)	Beam current (mA)	Beam efficiency (EAF)
CSTA-12-A	0.97858	1.49	13.34	18.09	82.97
CSTA-12-B	0.97889	1.37	14.33	19.44	77.16
CSTA-12-C	0.97862	1.29	15.42	20.92	71.69
CSTA-12-D	0.97825	1.55	13.02	17.66	84.95
CSTA-12-E	0.97855	1.45	13.72	18.61	80.60
CSTA-12-F	0.97854	1.44	13.87	18.81	79.75

Fig. 13 shows the axial distributions of power density of pins in FA in CSTA-12 schemes. Here, the power densities of pins in the same FA are averaged at the same axial position. It can be seen that the fuel power is symmetrically distributed in the axial direction. The highest power density located in the center of the fuel region. The maximum power density exceeding 750 W/cm^3 in the CSTA-12-A scheme which the CSTAs are close to the core center. In the CSTA-12-F scheme, the maximum power density is the lowest, about 550 W/cm^3 .

Fig. 14 shows the radial distribution of power density in fuel pins. In the uniform fuel scheme, the highest pin power density appears in the central FA of the core. In the fuel zoning scheme, the highest power of the fuel pin appears in the fuel pins closed to inner CSTA. Compared to the uniform fuel scheme, the power density in the central area decreased about $70\sim100 \text{ W/cm}^3$ and the pin power density near CSTA decreased by 50 W/cm^3 in the fuel zoning scheme.

The maximum power densities and the beam densities in different schemes are shown in Fig. 15. There is a slight change in the beam density for all CSTA-12 schemes, with the highest beam density in CSTA-12-C being $15.42 \mu\text{A}/\text{cm}^2$, and the lowest beam density in CSTA-12-D being $13.02 \mu\text{A}/\text{cm}^2$. However, there is a significant difference in the maximum power density among CSTA-12 schemes, with the highest power density of CSTA-12-A being 770 W/cm^3 , and the lowest fuel power density of CSTA-12-F being 601 W/cm^3 , with a difference of 170 W/cm^3 .

Based on the heat transfer limit of the spallation target window, the

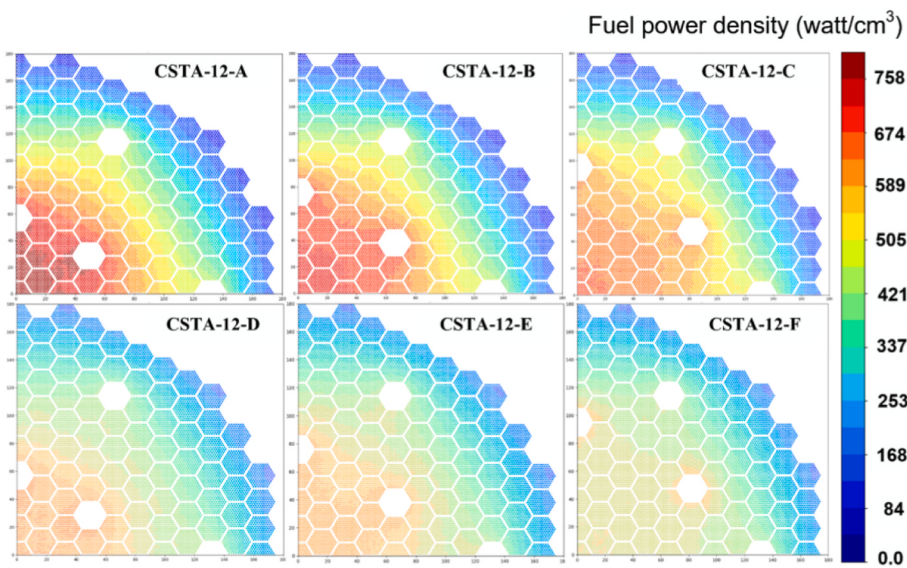


Fig. 11. Distribution maps of fuel pin power density in the CSTA-12 schemes.

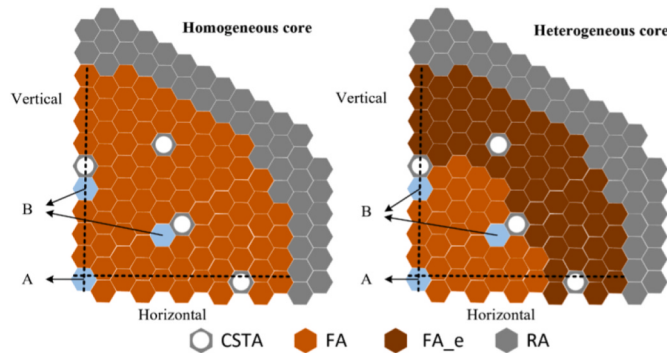


Fig. 12. Schematic diagram of statistical location of pin power distribution under the MB-ADS schemes.

beam density in most ADS designs ranges from $20\mu\text{A}/\text{cm}^2$ to $40\mu\text{A}/\text{cm}^2$. The beam density on the target window is relatively low, ensuring no target heat transfer difficulties arise among those CSTA-12 schemes. The maximum power density on the fuel pin not only affects the maximum temperature of the cladding and fuel pin during normal operation, but

also affects the design of residual heat removal system under accident conditions. Therefore, we prefer to choose the CSTA-12-F scheme with the most flat power distribution as the reasonable scheme.

3.4. The influence of neutron libraries

Based on the scheme of CSTA-12-F, the core k_{eff} has been simulated by OpenMC using different neutron libraries. ENDF/B-VII.1, ENDF/B-VIII.0, JEFF-3.3, JENDL-5 and JENDL-5+TENDL-2021 were applied in the simulations, and the results are shown in Fig. 16. It can be seen that the differences of simulated k_{eff} of ENDF/B-VII.1, ENDF/B-VII.0, and JEFF-3.3 are less than 100 pcm. The simulated k_{eff} using JENDL-5 is about 500 pcm higher than that of ENDF/B-III.0. The simulated reactivity of the mixed library JENDL-5+TENDL-2021 is 950 pcm higher than that of ENDF/B-III.0.

By adjusting the ratio of Pu and MAs in the nuclear fuel, the k_{eff} of the CSTA-12-F with different neutron libraries is adjusted to between 0.9780 and 0.9785. Since only a small number of nuclides in the neutron libraries have energy upper limits up to 200 MeV, and most of the energy upper limit is 20 MeV. We set the leaked neutron with energy above 20 MeV–20 MeV to ensure that the OpenMC can perform simulations. In the simulation using the mixed library JENDL-5+ TENDL-2021, the upper

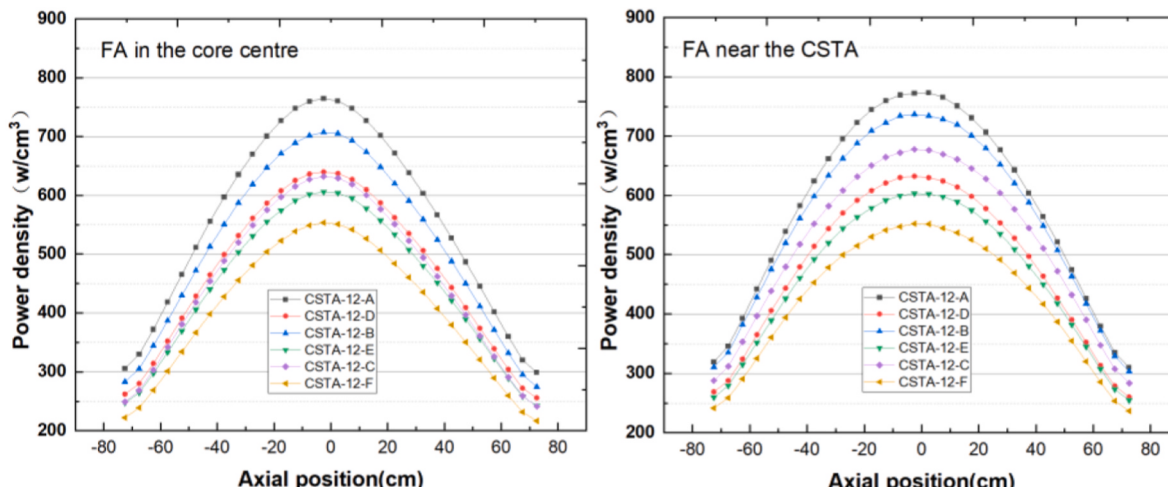


Fig. 13. Axial distribution of fuel pin power density.

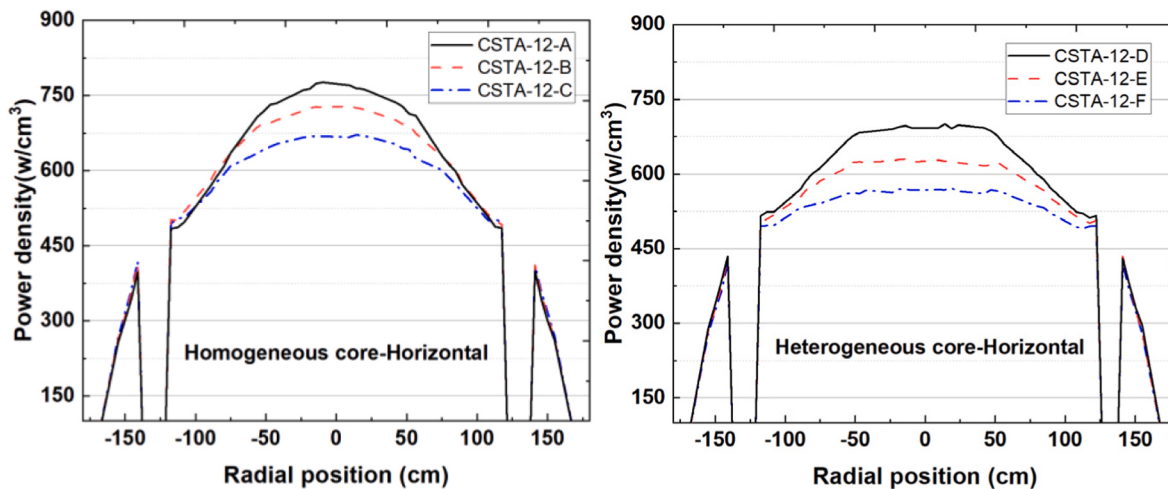


Fig. 14. Fuel pin power density distributions in horizontal and vertical.

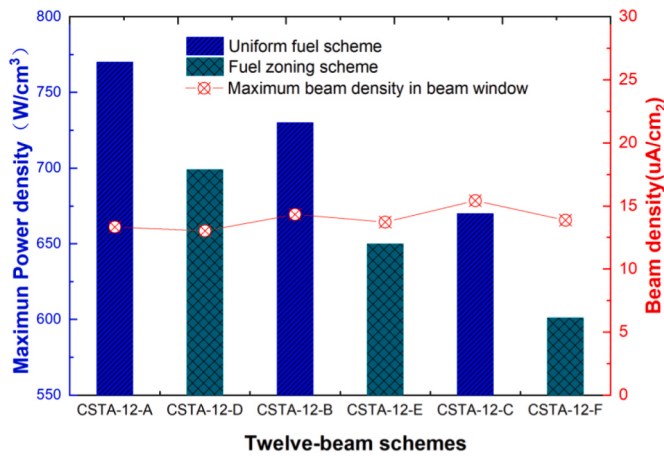


Fig. 15. Comparison of maximum core power density and beam density.

limits of the external neutron source were set to 200 MeV and 20 MeV respectively. The basic neutronic parameters of the CSTA-12-F under different libraries were obtained through simulations, and the results are shown in Table 8. In different sets with neutron energy upper limit of 20 MeV, the simulated neutron efficiency achieved good consistency, with the value of φ^* between 1.14 and 1.18. Therefore, the beam current and efficiency also obtained consistent results under different nuclear libraries, the difference is less than 5%. However, it is observed that the use of high energy neutron library results in a 24% increase in beam efficiency and a 20% decrease in beam current. High energy neutrons from external sources cannot be ignored in ADS research.

Fig. 17 shows the distributions of pin power density based on different nuclear libraries and neutron energy cutoff, and the tally range referring to the vertical direction in Fig. 12. The statistical error of the power density calculated by the OpenMC is less than 0.5%. It can be seen that the pin power density based on different neutron libraries is consistent, with a numerical difference of less than 4%. However, in the simulation based on the JENDL-5 + TENDL-2021 mixed library, the pin power density of in the core central region with neutron energy cutoff 200 MeV is about 30 W/cm³ higher than that with the neutron energy cutoff 20 MeV, with a difference of over 5%. The high-energy neutrons

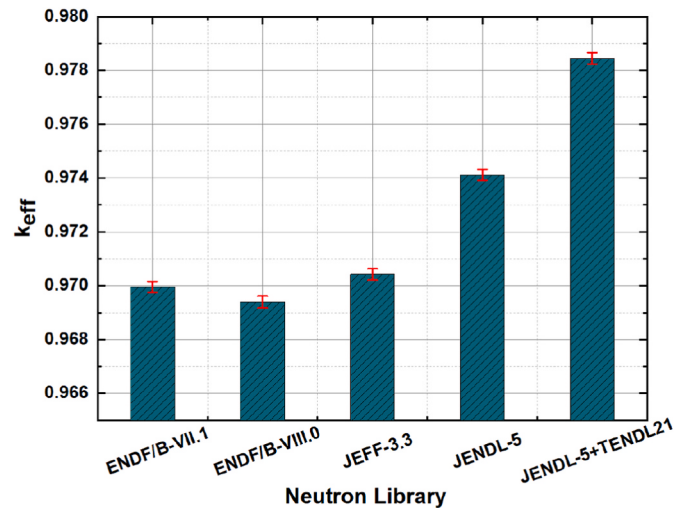


Fig. 16. Core k_{eff} calculated using different neutron libraries.

in external neutrons can also have an undeniable impact on the power distribution of subcritical reactor.

4. Conclusion

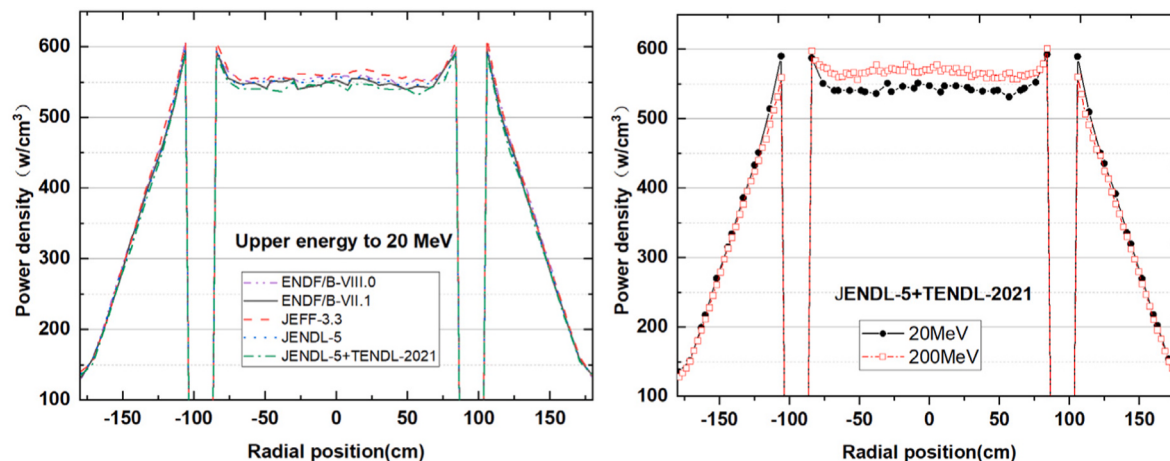
In the ADS scheme of one spallation target, the efficiency of the proton beam decreases with the increase of target diameter, and the maximum fuel power density also decreases with the increase of target diameter. The use of zoning strategy for nuclear fuel in the core is beneficial to reducing the maximum power density, but the beam efficiency is also reduced. Therefore, it is difficult to simultaneously balance the issues of the beam efficiency and the power flattening in one target ADS scheme.

In the optimization strategy of proton beam splitting into multi-beam bombarding multi-target to driven the driven sub-critical reactor, the spallation target is designed as a compact target assembly, and the proton beam is divided into a larger number of beamlets. Through optimization research on 6-beam and 12-beam, it is found that only when the CSTAs are arranged far from the central of the core can the power be

Table 8

The neutronic parameters of CSTA-12-F under different neutron libraries.

Library	Upper Energy(MeV)	k_{eff}	φ^*	Beam current (mA)	Beam efficiency (EAF)
ENDF/B-VII.1	20.00	0.97818	1.17	23.37	64.20
ENDF/B- VIII.0	20.00	0.97838	1.14	23.79	63.04
JEFF-3.3	20.00	0.97868	1.15	23.13	64.84
JENDL-5	20.00	0.97844	1.18	23.07	65.01
JENDL-5+TENDL-2021	20.00	0.97845	1.16	23.38	64.21
JENDL-5+TENDL-2021	200.00	0.97845	1.44	18.81	79.75

**Fig. 17.** The power distribution on the fuel pins calculated based on different neutron libraries and energy cutoffs.

effectively flattened. Compared with the results of one target ADS scheme, the reasonable MB-ADS scheme has advantages in both beam efficiency and core power flattening. The beam density on the target window is greatly reduced in the 12-beam scheme by using the fuel zoning strategy. This is a characteristic that the one source ADS can not be achieved. There is a significant impact on the beam efficiency and affects power distribution with the high energy neutron in libraries. Comprehensive cross-section libraries of high-energy neutron are required for the research and design of ADS.

The MB-ADS uses multiple CSTAs to drive the subcritical reactor. A small target diameter reduces the leakage rate of neutrons in the direction of beam recoil, and the proportion of high-energy neutrons in external neutrons is greatly increased. There is no dedicated loop or active component for targets, and the accelerator is directly coupled with the sub-critical reactor. By dispersing the beam density through multiple CSTAs, the heat transfer problem of target window and material damage is expected to be reduced. CSTAs can be flexibly distributed at different positions in the core. The ADS designers can search for suitable numbers and positions of CSTAs to optimize system parameters.

CRediT authorship contribution statement

Xunchao Zhang: Writing – original draft, Methodology, Investigation, Data curation, Conceptualization. **Neng Pu:** Writing – review & editing, Investigation, Data curation. **Huan Jia:** Writing – review & editing, Validation, Formal analysis. **Yuanshuai Qin:** Writing – review & editing, Methodology, Formal analysis. **Hanjie Cai:** Writing – review & editing, Visualization, Validation. **Yuan He:** Writing – review & editing, Supervision, Project administration, Funding acquisition.

Declaration of competing interest

The authors declare that they have no known competing financial interests or personal relationships that could have appeared to influence the work reported in this paper.

Acknowledgement

This work is funded by Large Research Infrastructures - China initiative Accelerator Driven System (2017-000052-75-01-000590). The China Initiative Accelerator Driven System (CiADS) is a major scientific and technological infrastructure prioritized for construction during the 12th Five Year Plan period in China. CiADS will be the world's first megawatt level accelerator driven subcritical system principle verification device, enabling China to comprehensively master the key technologies involved in accelerator driven subcritical systems and gain experience in system integration and operation.

Data availability

Data will be made available on request.

References

- Abderrahim, Hamid Ait, Baeten, Peter, De Bruyn, Didier, Fernandez, Rafael, 2012. MYRRHA-A multi-purpose fast spectrum research reactor. *Energy Convers. Manag.* 63 (2012), 4–10.
- Ali, Ahmad, Steven, J. Steer, Parks, Geoffrey T., 2013. A preliminary study of target multiplicity for ADSRs. *Energy Convers. Manag.* 69, 181–190, 2013.
- Bokova, T.A., Meluzov, A.G., Bokov, P.A., Volkov, N.S., Marov, A.R., 2021. Variants of nuclear power plants of small and medium power with heavy liquid-metal coolants. *Open J. Microphys.* 11, 53–71.
- Conlin, Jeremy Lloyd, 2019. Development and maintenance of NJOY. United states. Web: <https://doi.org/10.2172/1493523>.
- Dagan, R., Broeders, C.H.M., 1999. Optimization of multiple source system for ADS. In: *20th Conference of Nuclear Societies in Israel. Dead Sea; 1999*.
- Gohar, Y., Finck, Krajt, P., Herceg, L., Pointer, J., Saiveau, W., Sofu, J., Hanson, T., Todosow, Albert, Koplow, Michael, Mijatovic, M., Panto, 2002. Lead-Bismuth Target Design for the Subcritical Multiplier (SCM) of the Accelerator Driven Test Facility (ADTF). <https://doi.org/10.2172/7797950>.
- Gohar, Yousy, Cao, Yan, Kraus, Adam R., 2021. ADS design concept for disposing of the U.S. spent nuclear fuel inventory. *Ann. Nucl. Energy* 160, 108385, 2021.
- Iwamoto, O., Iwamoto, N., Kunieda, S., Minato, F., Nakayama, S., Abe, Y., et al., 2023. Japanese evaluated nuclear data library version 5: JENDL-5. *J. Nucl. Sci. Technol.* 60 (1), 1–60.
- Koning, A.J., Rochman, D., Sublet, J., Dzysiuk, N., Fleming, M., van der Marck, S., 2019. TENDL: complete nuclear data library for innovative nuclear science and technology. *Nucl. Data Sheets* 155.

- Mansani, L., Artioli, C., Schikorr, M., Schikorr, Rimpault, G., Angulo, C., Debruyn, D., 2012. The European lead-cooled EFIT Plant: an Industrial-Scale accelerator-driven system for minor actinide transmutation. *Nucl. Technol.* 180, 241–226.
- Pignatello, J.-F., Richard, P., Rimpault, G., Murgatroyd, J., Stainsby, R., Schikorr, M., Bubelis, M., Larmignat, S., Woaye-Hune, A., Ridikas, D., Takabayev, A., 2012. Description of the European Helium Cooled EFIT Plant: an industrial-scale accelerator-driven system for minor actinide transmutation. *Nucl. Technol.* 180, 264–296.
- Pu a, Neng, Zhang, Xun-Chao, Cai, Han-Jie, Jia, Huan, Liang, Tian-Jiao, Yuan, He, 2023. Evaluation of OpenMC calculations coupling with PHITS, FLUKA, and GEANT4 for ADS study. *Prog. Nucl. Energy* 155 (2023), 104505.
- Romanoff, Paul K., Horelik, Nicholas E., Herman, Bryan R., Nelson, Adam G., Forget, Benoit, Smith, Kord, 2015. OpenMC: a state-of-the-art Monte Carlo code for research and development. *Ann. Nucl. Energy* 82, 90–97.
- Sato, T., et al., 2018. Features of particle and heavy ion transport code system (PHITS) version 3.02. *J. Nucl. Sci. Technol.* 55, 684–690.
- Keijers, Steven, 2014. Evolution of the MYRRHA Spallation target design from windowless loop to loopless window. MEGAPIE Final Technical Review Meeting , October 2014, Bregenz, Austria. https://indico.psi.ch/event/3182/images/699-04_S.Keijers_Evolution_MYRRHA_Spallation_Target_Design.pdf.
- Sugawara, Takanori, Eguchi, Yuta, Obayashi, Hironari, Iwamoto, Hiroki, Tsujimoto, Kazufumi, 2018. Conceptual design study of beam window for accelerator-driven system with subcriticality adjustment rod. *Nucl. Eng. Des.* 331 (2018), 11–23.
- Tsujimoto, K., Sasa, T., Nishihara, K., Oigawa, H., Takano, H., 2004. Neutronics design for lead-bismuth cooled accelerator-driven system for transmutation of minor actinide. *J. Nucl. Sci. Technol.* 41–1, 21–36.
- Zhang, Xunchao, Lin, Yu, Yan, Xuesong, Zhang, Yaling, Cai, Hanjie, Li, Jianyang, Zhang, Zhilei, Chen, Liangwen, Gao, Xiaofei, Yang, Lei, 2019. The optimization on neutronic performance of the granular spallation target by using low-density porous tungsten. *Nucl. Instrum. Methods Phys. Res. Sect. A Accel. Spectrom. Detect. Assoc. Equip.* 916, 22–31.
- Zheng, Y.Q., Li, X.Z., Wu, H.C., 2017. Effect of high-energy neutron source on predicting the proton beam current in the ads design. *Nucl. Eng. Technol.* 49 (8), 1600–1609.